https://doi.org/10.48048/tis.2023.5472

Molecular Modeling, Docking, and QSAR Studies on A Series of N-arylsulfonyl-N-2-pyridinyl-piperazines Analogs Acting as Anti-Diabetic Agents

Ajita Paliwal*, Smita Jain and Sarvesh Paliwal

Department of Pharmacy, Banasthali Vidyapith, Rajasthan 304022, India

(*Corresponding author's e-mail: ajitapaliwal19@gmail.com)

Received: 2 August 2022, Revised: 12 September 2022, Accepted: 19 September 2022, Published: 19 March 2023

Abstract

The Molecular structure of compounds contains a lot of information that can be used further. A classical Quantitative Structure Activity Relationship (QSAR) method was used to decode that information based on the descriptors. The study was performed on a mono-substituted series of Glucokinase-Glucokinase regulatory protein inhibitors (GK-GKRP/GCKR). A sequential application of the statistical method, both linear and nonlinear, has been used in the study which includes Multiple Linear Regression (MLR), Partial Least Square (PLS), and Artificial Neural Network (ANN). The developed model was validated using various statistical methods to evidently prove its reliability and precision. This knowledge will be used to design a new compound. Docking studies will be performed to establish the binding pattern of the designed compound. The prophetic power and robustness of the model containing 26 compounds in the training set were proven by the various statistical parameter s value: 0.30, F-value: 41.8, r: 0.94, r^2: 0.88, r^2CV: 0.77. The model gives insight into the various descriptors that are selected for the present study. The present study not only shows the contribution of various substituents in the biological activity but also indicates the changes that can be done to design the new potent molecules with more selectivity and less toxicity.

Keywords: Glucokinase-Glucokinase regulatory protein (GK-GKRP/GCKR), Quantitative Structure Activity Relationship (QSAR), Docking, Multiple Linear Regression (MLR), Partial Least Square (PLS), Artificial Neural Network (ANN)

Introduction

The prevalence of type 2 diabetes is increasing worldwide and it is estimated that by the year 2025 nearly 300 million people will be suffering from diabetes. Diabetes brings with it other metabolic disorders and other complications like retinopathy, neuropathy, nephropathy, and peripheral and vascular insufficiencies. The enhancement in the number of cases of type 2 diabetes has been majorly due to a sedentary lifestyle and less physical activity. Insensitivity to insulin or changes in the level of insulin is the major cause of type2 diabetes that results in an increased in blood sugar levels.

Glucokinase is one of the hexokinase isoenzymes that is responsible for the entry of glucose into the glycolytic pathway. The liver and pancreas are the 2 major sources of insulin for the body. In liver and pancreatic beta cells glucokinase is present that converts glucose to glucose-6-phosphate in pancreas. In the pancreas GK is the rate-limiting enzyme for insulin secretion. In liver, it follows Non-Michaelis-Menton kinetics (CGGTM). Direct activation of Glucokinase in the pancreatic cells has shown to induce hypoglycemia due to over activation. Allosteric activation of GKs has been shown to decrease the glucose level without any hypoglycemia [1]. Structural insights into GK have shown that it consists of 2 domain that is large and small and occur in 3 state i.e. wide open (inactive), super open, and closed (active). These large and small domains undergo transitional changes from active to inactive states [2].

In liver the GK activity is maintained by the protein called as Glucokinase Regulatory Protein (GKRP). This GKRP remains bound to GK as GKRP-GK complex, during inactive super open conformation of GK. This GKRP-GK complex is glucose dependent, so GKRP sequester GK in the nucleus during fasting conditions. As the blood sugar level raises this complex disrupts to release of the GK. The unbound GK will translocate to the cytoplasm to facilitate the metabolism of glucose by converting the glucose to glucose-6-phosphate, the very first step of the glycolytic pathway [3,4].

Targeting this protein in a manner to disrupt the complex will not affect the kinetics of the enzyme and hence the risk to cause any hypoglycemia can be lowered [5]. In the present study, the Insilco tools of qualitative structure activity relationship for drug discovery will be utilized to develop the new drug entities. Various methods of *in silico* drug design like MLR, PLS, and ANN will be used to predict the activity of the compound.

Material and methods

Dataset for analysis

An aryl series of 40 compounds having good log IC50 values is selected from the literature. Generally, the reported activities are skewed so the biological activity is taken as −log of the given IC50 value by using the following formula:

$$pIC50 = -\log IC50$$

Sketching of the compounds available in the series is done by using the chemDraw ultra 8.0 software ((https://www.perkinelmer.com), USA) [6]. Structure cleanup is applied to avoid any mistakes in the structure (bending or stretching). Moving towards the QSAR development the structures were then used for further study by importing them into the new data sheet of TSAR 3.3 (https://www.accelrys.com) [7].

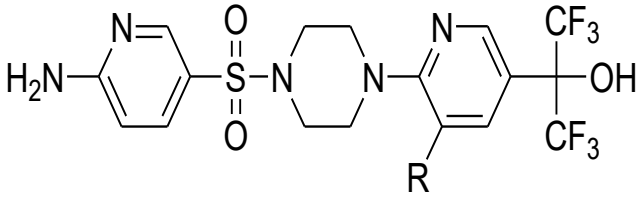

Define substituent and dataset preparation

The series at hand has only 1 substitution, around the pyridyl ring (whole series). The substituents were defined by using the "define substituent" option in-built in the TSAR worksheet (version 3.3; Accelrys Inc., Oxford, England) as shown in **Figure 1**. The structure was then converted into high quality by using CORNIA-Make 3D [8]. Then the COSMIC option was employed to determine the total energy of the molecule, which is the sum of torsion angle, Vander walls force, columbic force, etc.

Calculating descriptors

After importing structure, defining substituent, and minimizing energy the next step is to calculate the descriptor and then refine them to select only those that are much or closely correlated to the biological activity. Nearly 200 classical descriptors from the geometrical, structural, electronic, and hydrophobic classes were generated by calculating their statistical values using the whole molecule along with substituent. Various descriptors like kier chi, kappa, dipole moment, molecular, indices, HOMO, LUMO, logP, and other molecular, electronic, topological descriptors and VAMP were obtained using the TSAR package [9].

Data reduction

Data redundancy, which is the main cause of deceptive results, is mainly observed when the data are large and lead to ambiguity in choosing the relevant descriptors. So, the Correlation matrix is used to limit and refine the data and to obtain the most correlated descriptor or physicochemical parameter with biological activity and no intercorrelation. While performing the correlation matrix pairwise correlation method was used for the evaluation of the descriptors. Descriptors that highly correlate with biological activity were retained [10]. These descriptors are used for performing correlation and then used in the final model building and are used to interpret the information that is encoded in the structure of the molecules.

Statistical analysis

To statistically analyze the data various regression methods were applied to form and validate the model. The whole series was divided into test and the training set. The training set compounds are utilized to generate the model while the test set compounds were used to internally validate the model developed

by training set molecules. Regression analysis was carried out through the execution of MLR, PLS, and ANN options, accessible in TSAR 3.3. The assessment of the predictive power of the anticipated model was performed and confirmed through a set of statistical parameters, such as standard deviation (*s*), squared regression coefficient (*r*2), conventional regression coefficient (*r*), cross-validation test (*r*2cv), and Fischer's ratio (*F*) [11].

Multiple linear regression analysis (MLR)

MLR describes the relationship between the biological activity data (dependent Y variable) and the structural descriptors (the independent X variable) using statistical calculation. MLR involves fitting the data, extracted from both the variables to the derived regression equations [12].

Partial least square (PLS)

PLS analysis method also explains the relationship between a dependent variable and a set of descriptors (independent variables) using the calculation of the equations. PLS is considered as a preferred tool for surmounting the difficulties of MLR, owing to redundancy resulted due to a large pool of data or high inter-correlations among descriptors [13].

Artificial neural network approach (ANN)

ANN is characteristically a software-based program that is designed to replicate like the human brain to analyze and process information. In the ANN technique, several neurons (the processing elements) are linked to each other through links like the net and form "layers." The features of the ANN are appropriate for the processing the data, particularly when the functional relationship between the input and the output is not previously defined or is of a nonlinear type.

Model validation

For the cross-validation, Leave-one-out method was used and involved the deletion of 1 descriptor, at a time, and analyzing the data set values for the obtained model based on the remaining descriptors. The values of *r*2 and cross-validation, with the least prediction error, were chosen. Additionally, the test set compounds, not included in the building of the model, are used to determine the predictability of the designed QSAR model [14].

Result and discussion

For the selected series, nearly 200 descriptors were generated after Make 3D and minimizing energy. To eliminate data redundancy data reduction was done in a pairwise manner with the simultaneous checks on the correlation matrix. After deleting the descriptors that are badly or not showing good correlation only 4 descriptors were left that are DIPOLE MOMENT Y Component (W.M), KIER CHI 3 (cluster) index, KAPPA3 Index (W.M), and VAMP Polarization XZ (W.M). After getting the suitable descriptors the data was divided as training set and test set in the ratio of 60:40 respectively. Training set compounds were used for the development of a model to predict the activity by using MLR, PLS, and ANN. The test set compounds were used to validate the training set. Plots between the experimental and predicted activity was made to estimate the power of the predicted model. These plots can also be used for the search of outliers, if any, in the model [15].

The regression equation that is derived through the MLR technique on the training set compounds is as follows:

$$Y = 0.17664571 \times X1 - 1.1089879 \times X2 + 0.56819743 \times X3 - 0.065191962 \times X4 - 1.5867109$$

where, X1 = Dipole moment Y component (Whole molecule), X2 = Kier chi 3 cluster, X3 = Kappa 3 (whole molecule), and X4 = VAMP polarization XZ.

Table 1 Representing experimental activity data and the predicted activity values of the training set compounds, obtained from multiple linear regression analysis.

Name of Compound	Structure	Actual activity	Predicted MLR	Predicted PLS	Predicted ANN
(2)	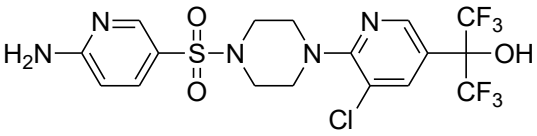	0.696804	0.827014	0.764481	0.880062
(3)	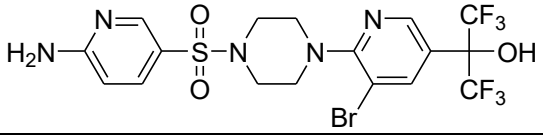	0.950782	0.842201	0.779327	0.880977
(6)	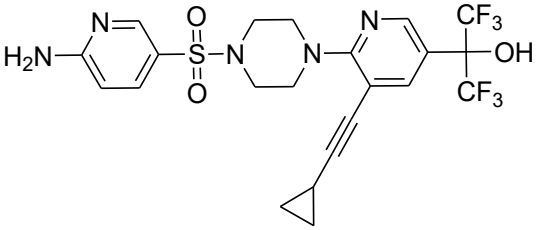	1.48149	1.79868	1.71616	1.67285
(8)	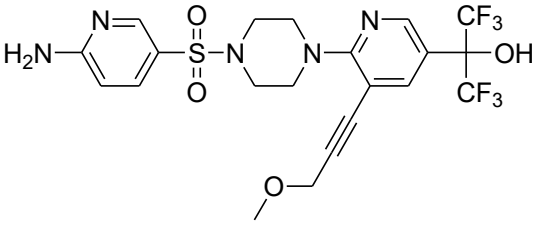	2.30103	2.63351	2.5926	2.32786
(9)	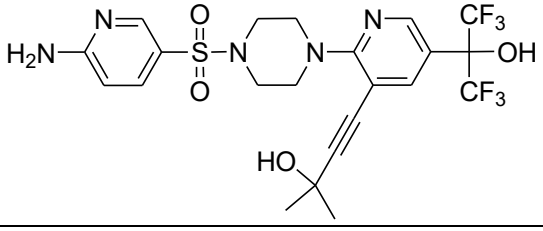	1.3098	1.04648	1.14274	1.24753
(10)	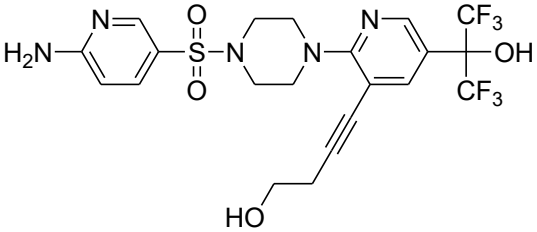	1.76955	2.06503	2.0761	1.89899
(11)	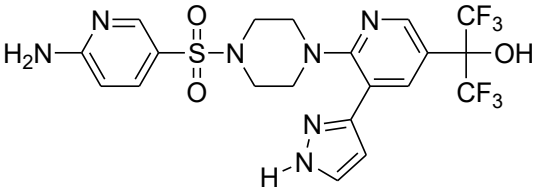	0.696804	0.181204	0.262399	0.65359
(12)	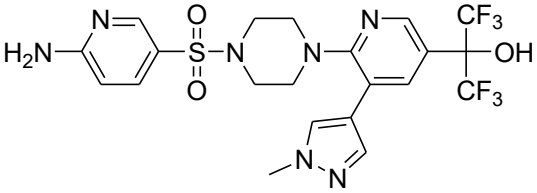	3	2.77023	2.64764	2.73791

Name of Compound	Structure	Actual activity	Predicted MLR	Predicted PLS	Predicted ANN
(15)	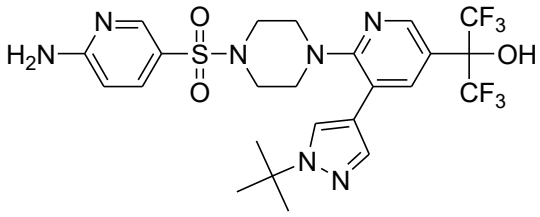	1.06048	0.732507	0.782764	0.917421
(17)	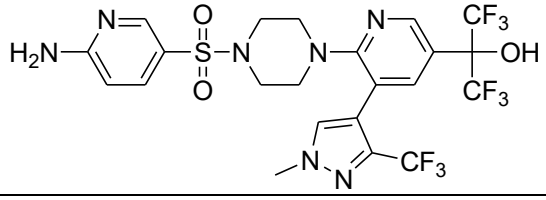	−1.47712	−0.710093	−0.54154	−1.39327
(19)	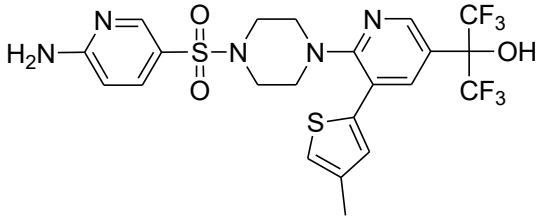	2.30103	2.20696	2.13192	2.25125
(20)	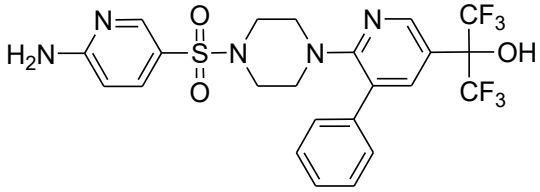	2.1549	2.20473	2.17231	2.09635
(23)	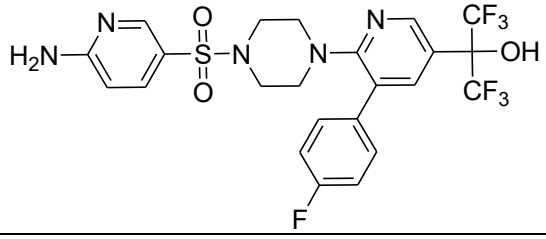	1.95861	1.90651	1.91539	1.87918
(24)	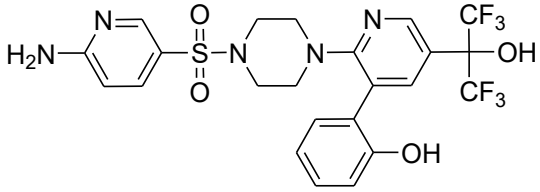	2.22185	1.92353	1.85192	1.81887
(25)	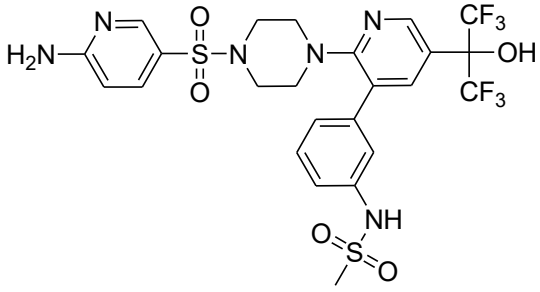	0.510042	0.374389	0.552811	0.286044

Name of Compound	Structure	Actual activity	Predicted MLR	Predicted PLS	Predicted ANN
(26)	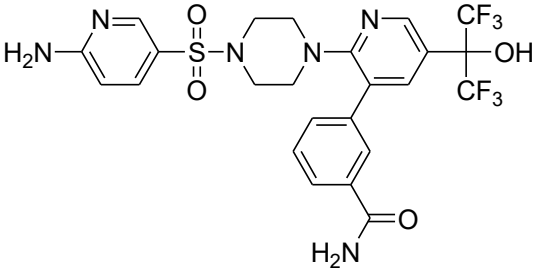	1.30103	1.36127	1.4144	1.49569
(27)	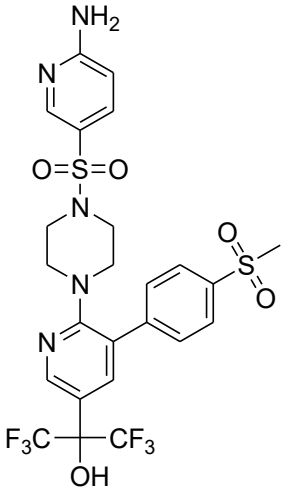	1.37675	1.13554	1.17703	1.44264
(29)	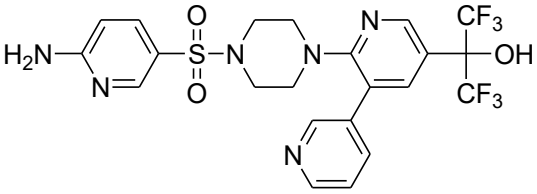	2.30103	2.35766	2.25387	2.09924
(32)	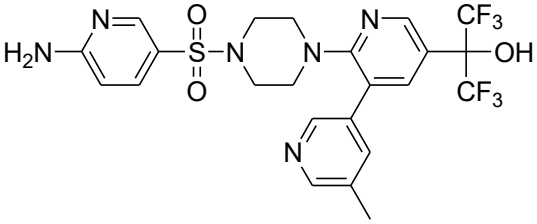	1.5376	1.51476	1.50586	1.56627
(33)	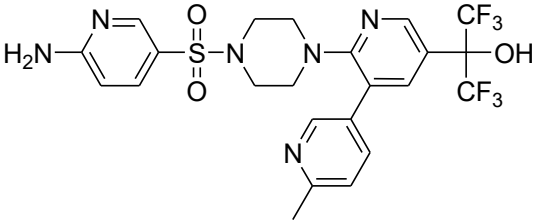	1.39794	1.58505	1.5695	1.60537
(34)	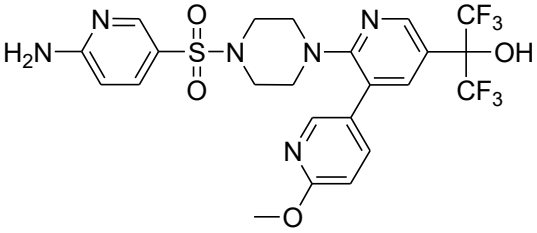	1.79588	1.32145	1.36423	1.54965

Name of Compound	Structure	Actual activity	Predicted MLR	Predicted PLS	Predicted ANN
(36)	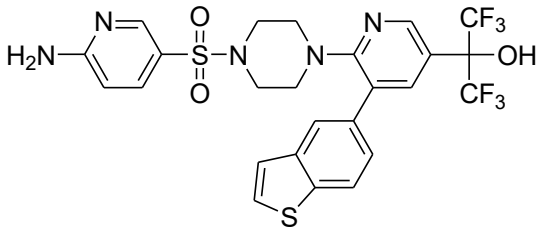	1.3279	1.37443	1.33276	1.46761
(37)	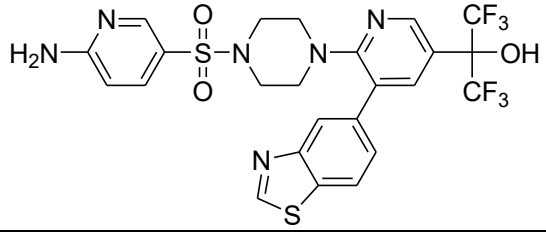	1.45593	1.57565	1.5846	1.53124
(38)	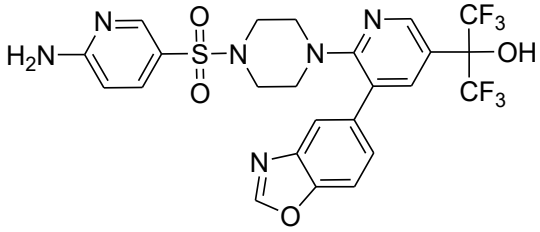	1.69897	1.7883	1.77781	1.78332
(39)	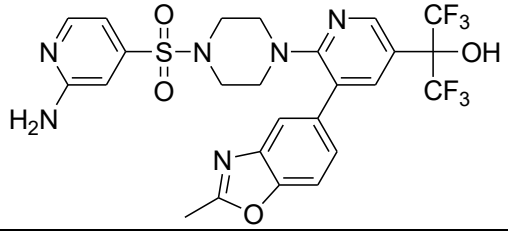	1.82391	1.91337	1.90089	2.05648
(41)	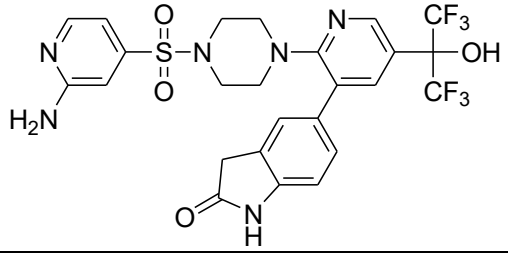	1.48149	1.70413	1.7065	1.78413

Table 2 Representing experimental activity data of the test set compounds and the predicted activity values, obtained through multiple linear regression.

Name of Compound	Structure	Actual activity	Predicted MLR	Predicted PLS	Predicted ANN
(1)	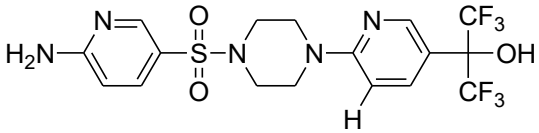	0.754487	0.374446	0.395263	0.769005
(4)	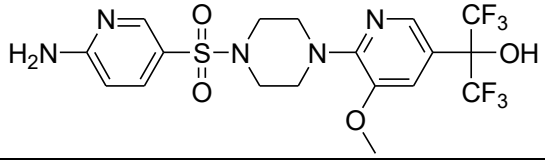	−0.045323	0.770249	0.671236	−0.01408

Name of Compound	Structure	Actual activity	Predicted MLR	Predicted PLS	Predicted ANN
(5)	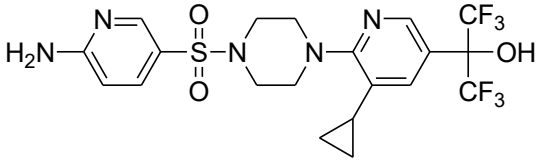	0.221126	0.18874	0.283391	0.179269
(7)	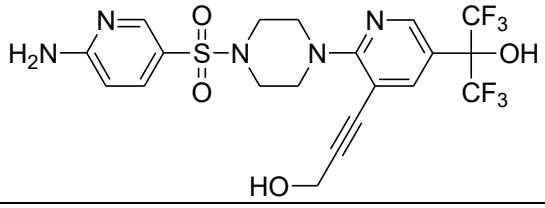	1.85387	1.75806	1.9812	1.95887
(13)	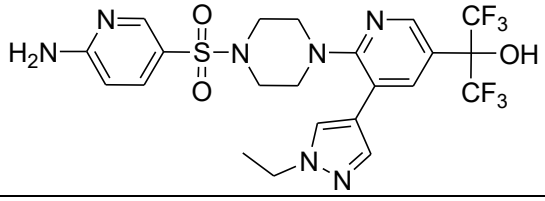	2.30103	1.66483	1.71092	1.95464
(14)	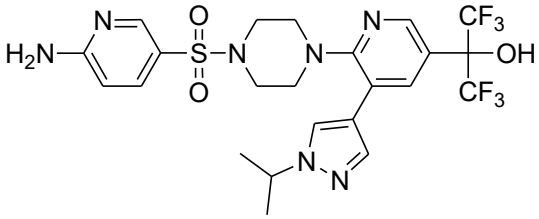	1.63827	1.96032	1.85098	1.73091
(16)	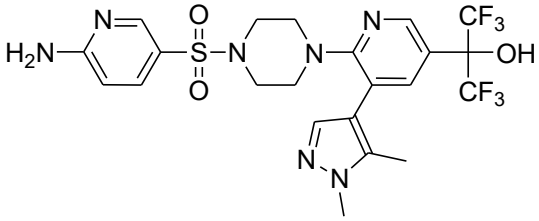	1.39794	1.31568	1.31699	1.42221
(21)	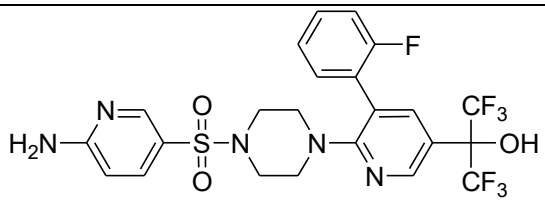	2.1549	1.66483	1.69173	1.94854
(22)	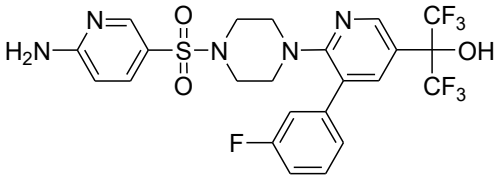	2.09691	1.84851	1.99838	1.8968
(28)	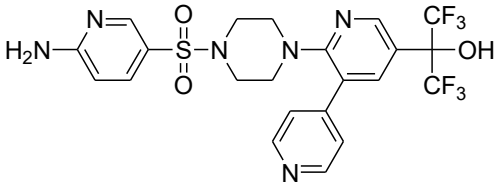	1.67778	1.56327	1.38856	1.5689

Name of Compound	Structure	Actual activity	Predicted MLR	Predicted PLS	Predicted ANN
(30)	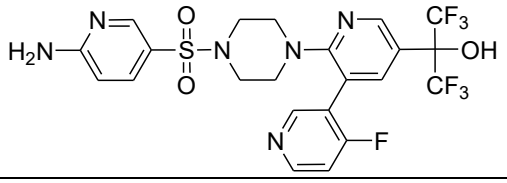	1.61979	1.66483	1.70859	1.95183
(31)	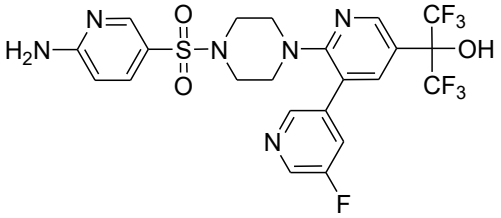	1.95861	1.84851	1.76708	1.93726
(35)	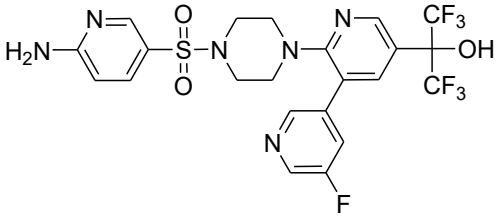	1.76955	2.14652	2.28514	1.96045
(40)	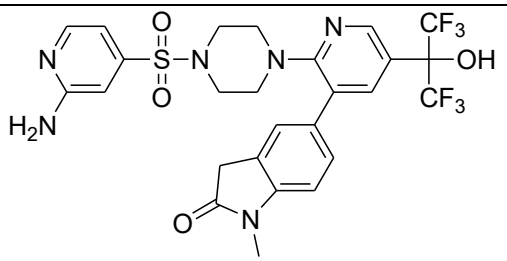	1.69897	1.78919	1.69564	1.55981
(42)	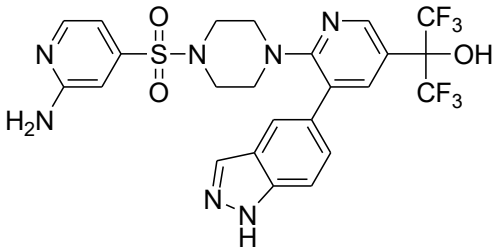	1.22185	1.54973	1.38624	1.20897
(44)	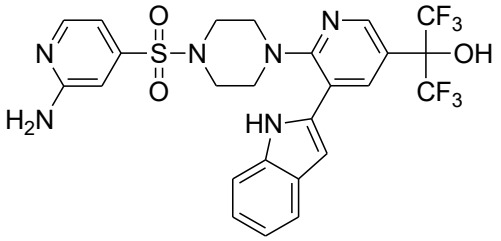	1.56864	1.54973	1.60121	1.93584
(45)	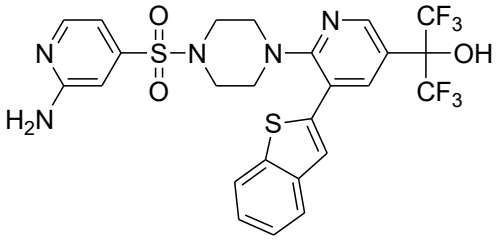	1.31876	1.54973	1.47462	1.59934

Table 3 Representing the values of standard parameters employed to evaluate predictability of the developed quantitative structure-activity relationship test model.

r	r^2	r^2Cv	*S*	*F*
0.83	0.70	0.59	0.36	35.44

As per the standard statistical value criterion, a minimal value of 0.80 for *r*2 is crucial for a statistically significant model [16,17]. Moreover, the developed model has an excellent *r*2 value of 0.88, yet once more proved the statistical significance of the model.

The robustness of the developed QSAR model was further evaluated by PLS and the equation is as follows:

$$Y = 1.276677 \times X1 - 0.26492366 \times X2 - 0.23346859 \times X3 - 2.4868717 \times X4 - 0.11788595 \times X5 - 4.7390904$$

The experimental versus predicted activity plots of training sets for MLR and PLS are shown in **Graphs 1** and **2** respectively. Captivatingly, regression values (R^2) of both the plots were enough close to validate the further reliability of the developed model.

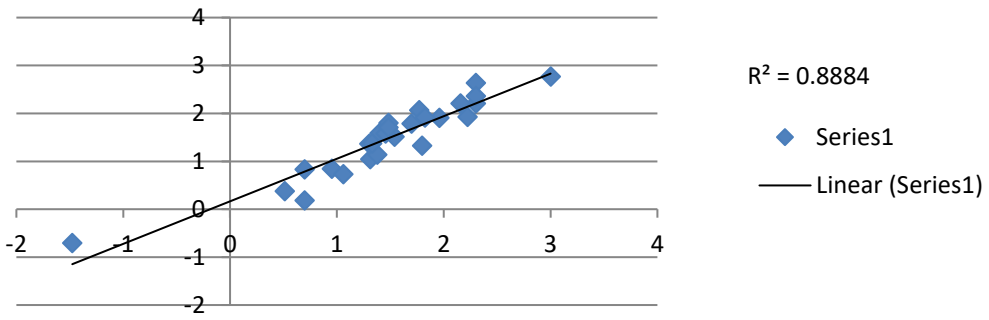

Graph 1 Graph of developed training model through MLR.

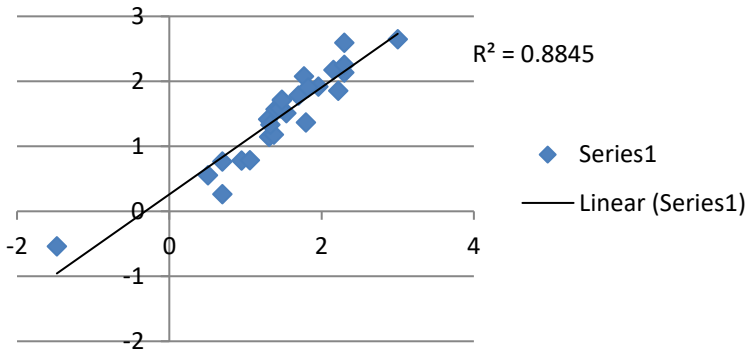

Graph 2 Graph of developed training model through PLS.

The experimental versus predicted activity plots of test sets for MLR and PLS is shown in **Graphs 3** and **4** respectively. This model validates the training set.

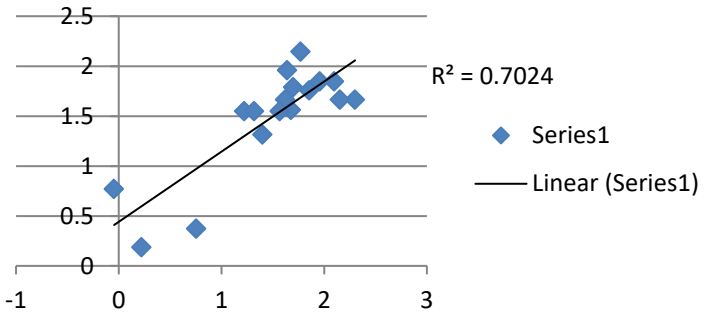

Graph 3 Graph of developed test model through MLR.

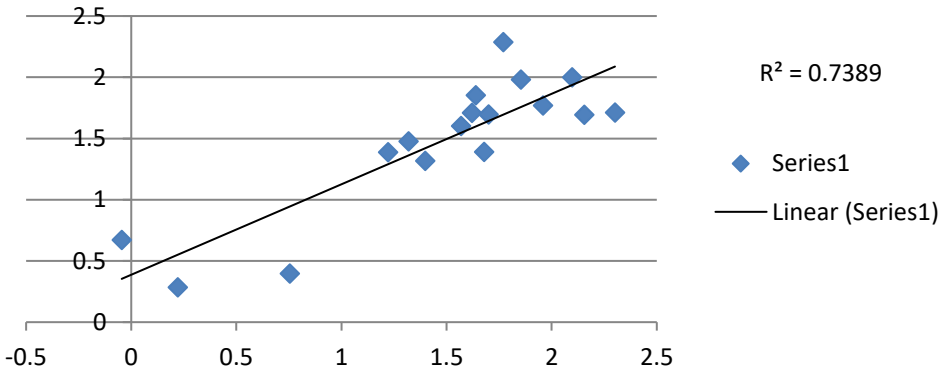

Graph 4 Graph of developed test model through PLS.

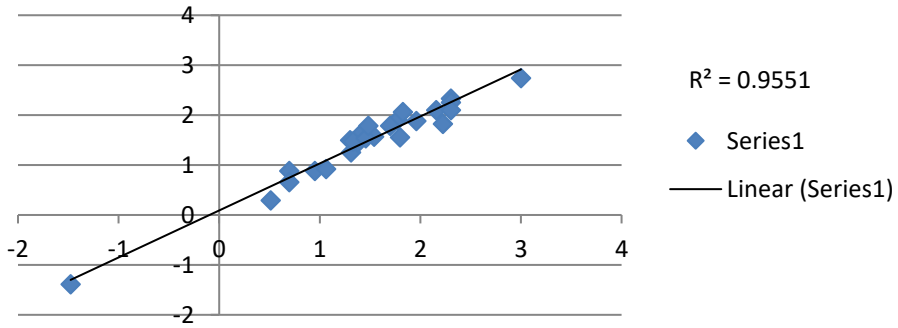

Graph 5 Graph of developed training model through ANN.

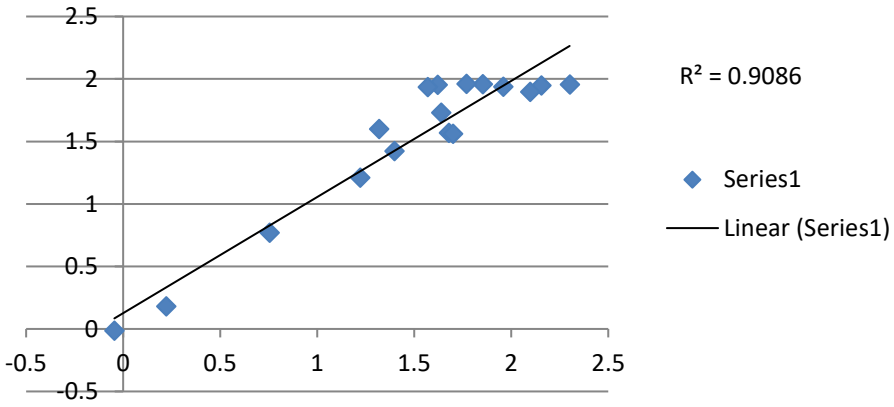

Graph 6 Graph of developed test model through ANN.

Table 4 Representing correlation matrix of derived descriptors and biological activity.

	−Log Ic50	**Dipole moment Y component (W.M)**	**Kier chi 3 cluster**	**Kappa 3 (W.M)**	**VAMP polarization XZ**
−Log Ic50	1	0.05206	0.23723	0.24742	0.57392
Dipole moment Y component (W.M)	0.05206	1	0.72629	0.13374	−0.55406
Kier chi 3 cluster	0.23723	0.72629	1	0.22675	−0.16383
Kappa 3 (W.M)	0.24742	0.13374	0.22675	1	−0.31646
VAMP polarization XZ	0.57392	−0.55406	−0.16383	−0.31646	1

The dipole moment Y component is a 3D electronic descriptor that indicates the strength and orientation behavior of a molecule in an electrostatic field. It describes the polarity of the molecule and is estimated by utilizing partial atomic charges and atomic coordinates. The dipole moment Y component is a 3D electronic descriptor that indicates the strength and orientation behavior of a molecule in an electrostatic field. It describes the polarity of the molecule and is estimated by utilizing partial atomic charges and atomic coordinates. The dipole moment y component describes the moments using the substituent point of attachment as an origin with this bond placed along the y-axis. It has been used to model polar interactions that contribute to the determination of the compound's lipophilicity as well as play an important role in drug-receptor interactions due to electrostatic effects. The dipole moment could influence electrostatic interactions with biological membranes. It explains molecular charge distribution on the y-axis and it is affected by the presence electronegative group.

Kier chi 3 cluster is topological descriptor, expressing molecular structure information at several levels of complexity. It is highly sensitive to changes in branching, and its value rapidly increases with the degree of branching.

Kappa 3 index is a molecular shape index based on assumption that shape of a molecule is a function of the number of atoms and their bonding relationship. Kappa 3 indicates the degree of branching at the center of a molecule.

VAMP Polarization XZ is a spatial descriptor that calculates the electronic properties of a compound and projects polarization towards XZ planes. There is a direct relation between polarizability and the number of valence electrons on every atom. It is a measure of weak intermolecular interaction & represents chemical reactivity at the XZ plane.

Table 5 Representing descriptor relevance for designed model.

Descriptor	Coffecient	Jacknife SE	Covariance SE	t Value	t probablity
Dipole moment Y component(W.M)	0.176646	0.0462942	0.0214324	8.24198	5.09E - 08
Kier chi 3 cluster	−1.10899	0.301195	0.151894	−7.30104	3.45E - 07
Kappa 3 (W.M)	0.568197	0.20836	0.177412	3.20271	0.00427657
VAMP polarization XZ	−0.065192	0.0119232	0.0110497	−5.89987	7.42E - 06

To deal with the nonlinear data and to further validate our findings of MLR, the ANN method was used. The neural network was used to train the developed model and to predict the activity data. The plots between original and predicted data are shown in the graphs below.

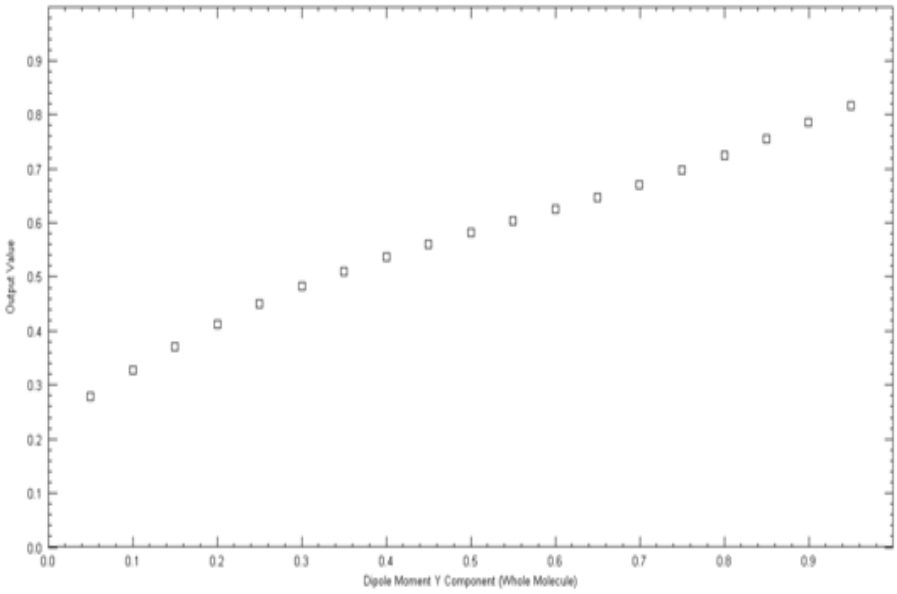

Figure 1 Neural graph of Dipole moment Y component (Whole Molecule) with biological activity.

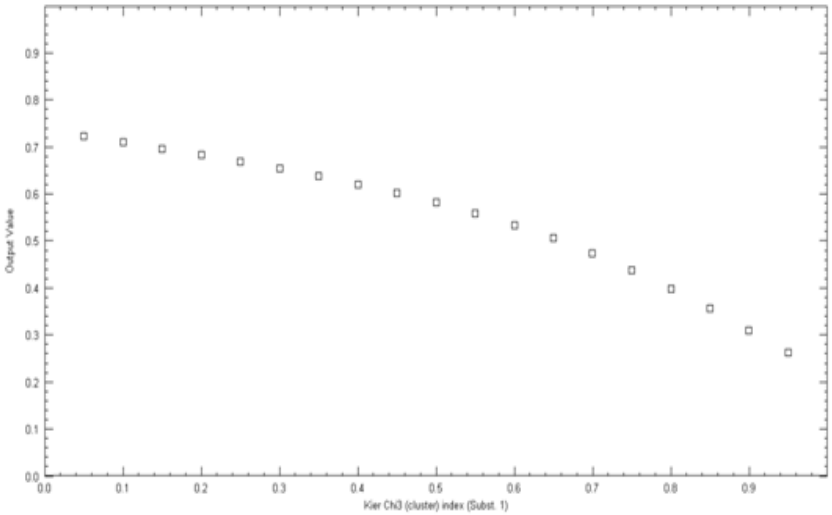

Figure 2 Neural graph of Kier chi 3 (cluster) index (subs 1) with biological activity.

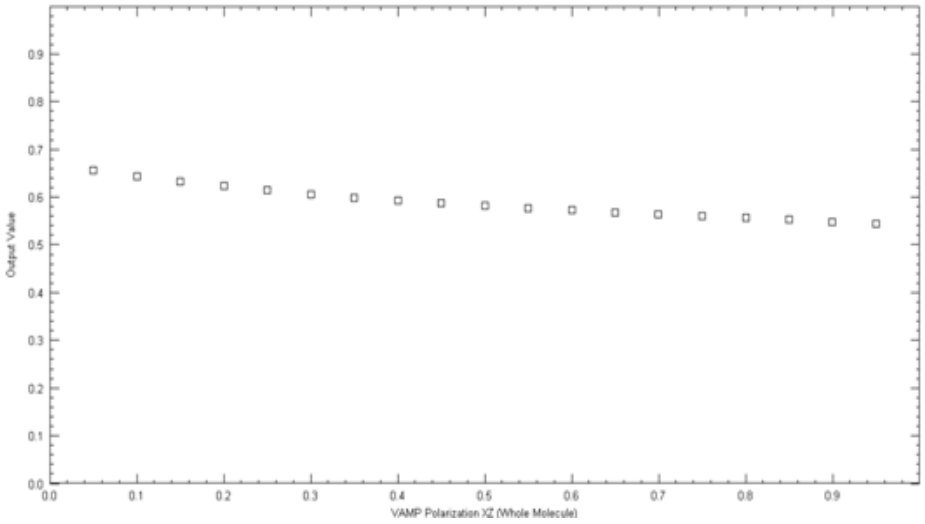

Figure 3 Neural graph of VAMP polarization XZ (Whole Molecule) with biological activity.

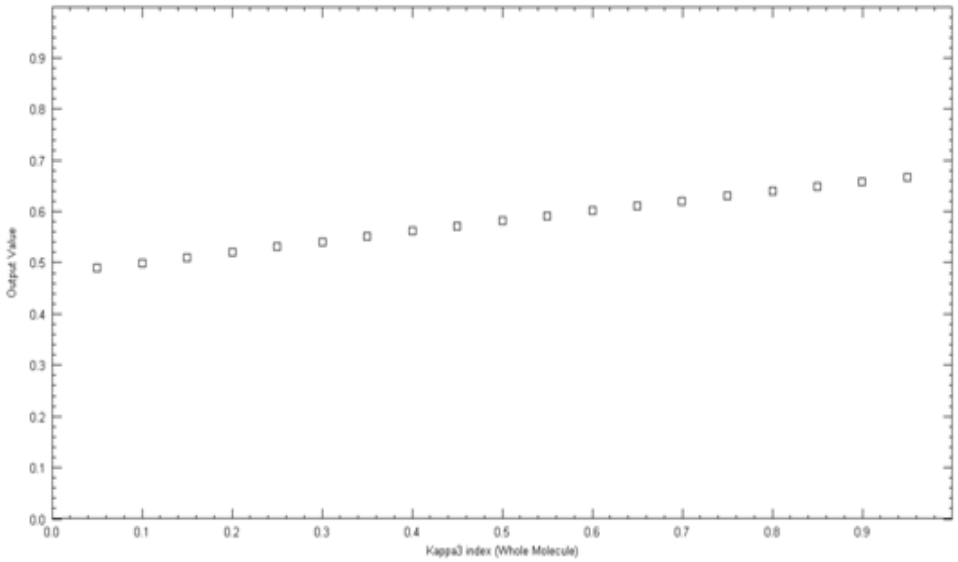

Figure 4 Neural graph of Kappa 3 index (Whole Molecule) with biological activity.

As seen in the above graphs and equation Dipole moment Y component (Whole molecule) and Kappa 3 (whole molecule) are showing a positive correlation with biological activity. And Kier chi 3 cluster and VAMP polarization XZ are negatively correlated. This signifies that an increase in values of X1 & X3 will increase the biological activity and vice versa, whereas for X2 & X4 when values decrease biological activity will increase.

The values of R^2 obtained from ANN are close enough to the one obtained from the MLR and PLS. This further validates the developed model. As reflected by the coefficient, jackknife values, covariance, t-values, and t-probability values that the descriptors taken into the study are of relevance. Their individual significance can is further established by the correlation of the descriptor with the biological activity.

Designing of the new optimized molecule

Designing a new chemical structure that contains all the distinct features in the requisite arrangement so as to attain the most efficient binding pattern with the target protein is a challenging task. After developing a QSAR model, some valuable insight into the molecular structure that is required for biological activity was gained. This retrieved information was used to design the compounds. A total of 10 compounds were designed (not reported here), the best fitted compound (A1) is shown below in **Figure 5**.

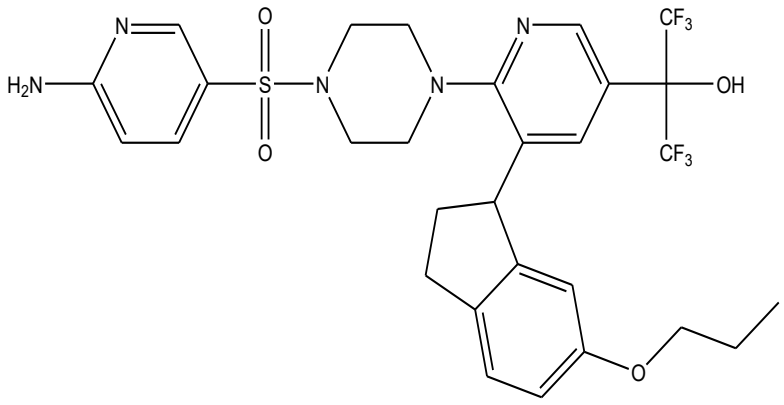

Figure 5 Structure of newly designed most potent compound (A1).

Docking

The designed novel compound was then used for docking study to further check the binding efficiency of the compound using PDB, 4OHM. Lib dock module from Discovery studio 2.0 was used to perform docking studies. All water molecules and side chains were removed from the PDB structure in a radius of 10Å. The top scored pose is used for analyzing polar and nonpolar interactions [18]. The complete docked structure of S1 and A1 is shown in **Figures 6** and **7**. For comparison the documented structure (S1) was also docked on the same PDB ID, to check the common amino acids and their binding to the defined protein. Compound A1 is showing interaction with the same amino acids as that of the documented compound S1. As seen in the docking picture below A1 is showing 1 hydrogen bonding (Dark green line) and 4 hydrophobic (pink line) interactions with the protein along with 7 carbon-hydrogen bond (light green lines) and 1 pi-anion interaction (orange lines). The amino acids in common are Gly 181, Agr 215, Val 28, Glu 32, Lys 514, and Pro 29 [19-23].

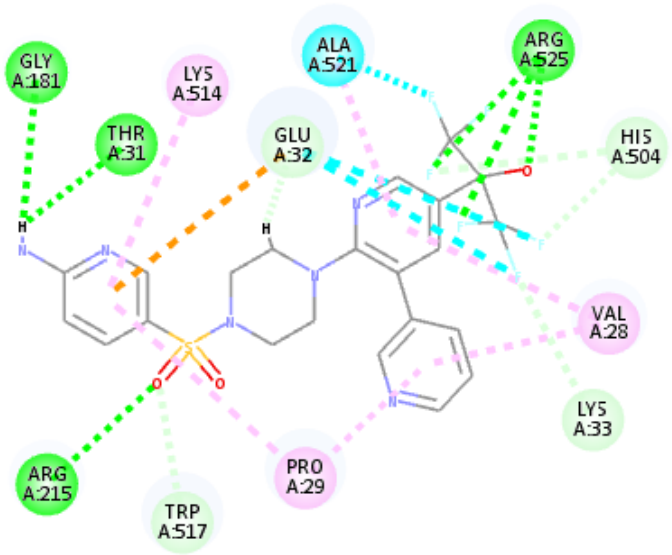

Figure 6 Docked picture of S1 on PDB 4OHM.

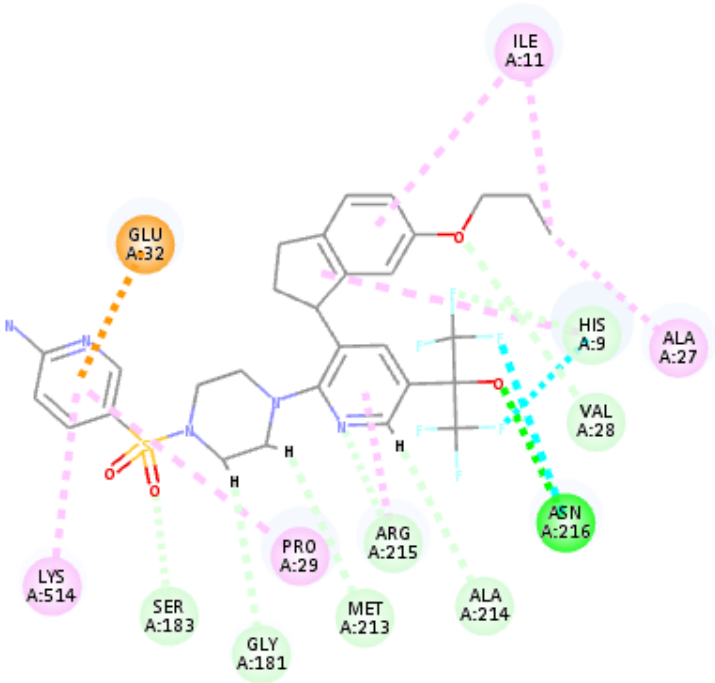

Figure 7 Docked picture of A1 on PDB 4OHM.

Conclusions

A Validated 2D QSAR model constituted with 4 descriptors, namely Dipole moment Y component (Whole molecule), Kier chi 3 cluster, Kappa 3 (whole molecule) and VAMP polarization XZ, was developed, and further validated to obtain knowledge about the dependence of biological activity on the molecular structure. In the defined study, the values of r, r^2, r^2cv, f-value, and s-value proved the statistical soundness of the model. The valuable information retrieved from this model can be used further to design and optimize the new compounds in terms of potency and selectivity. The docking study of the designed compound suggested hydrogen bonding with the enzyme pocket, which is essential for biological activity.

References

[1] FT Hong, MH Norman, KS Ashton, MD Bartberger, J Chen, S Chmait, R Cupples, C Fotsch, SR Jordan, DJ Lloyd and G Sivits. Small molecule disruptors of the glucokinase-glucokinase regulatory protein interaction: 4. Exploration of a novel binding pocket. *J. Med. Chem.* 2014; **57**, 5949-64.

[2] E Ermakova and R Kurbanov. Molecular insight into conformational transformation of human glucokinase: Conventional and targeted molecular dynamics. *J. Biomol. Struct. Dynam.* 2020; **38**, 3035-45.

[3] A Pautsch, N Stadler, A Löhle, W Rist, A Berg, L Glocker, H Nar, D Reinert, M Lenter, A Heckel and G Schnapp. Crystal structure of glucokinase regulatory protein. *Biochemistry* 2013; **52**, 3523-31.

[4] K Chen, K Michelsen, RJM Kurzeja, J Han, M Vazir, DJSJ Jr, C Hale and RC Wahl. Discovery of Small-Molecule Glucokinase Regulatory Protein Modulators That Restore Glucokinase Activity. *SLAS Discov.* 2014; **19**, 1014-23.

[5] H Watanabe, Y Inaba, K Kimura, M Matsumoto, S Kaneko, M Kasuga and H Inoue. Sirt2 facilitates hepatic glucose uptake by deacetylating glucokinase regulatory protein. *Nat. Comm.* 2018; **9**, 30.

[6] LD Mendelsohn. ChemDraw 8 Ultra, windows and macintosh versions. *J. Chem. Inform. Model.* 2004; **44**, 2225-6.

[7] Icon Group Ltd. *Oxford Molecular Group PLC: International competitive benchmarks and financial gap analysis (financial performance series)*. Icon Group International, Inc. California, 2004.

[8] A Dalby, JG Nourse, WD Hounshell, AK Gushurst, DL Grier, BA Leland and J Laufer. Description of several chemical structure file formats used by computer programs developed at molecular design limited. *J. Chem. Inform. Comput. Sci.* 1992; **32**, 244-55.

[9] A Nagpal and S Paliwal. Discovery of novel and selective c-jun nh2-terminal kinases 2 inhibitors by two-dimensional quantitative structure-activity relationship model development, molecular docking and absorption, distribution, metabolism, elimination prediction studies: An *in silico* approach. *Asian J. Pharmaceut. Clin. Res.* 2018; **11**, 100-8.

[10] R Arya, SP Gupta, S Paliwal, S Kesar, A Mishra and YS Prabhakar. QSAR and molecular modeling studies on a series of pyrrolidine analogs acting as BACE-1 Inhibitors. *Lett. Drug Des. Discov.* 2019; **16**, 746-60.

[11] K Roy and AS Mandal. Development of linear and nonlinear predictive QSAR models and their external validation using molecular similarity principle for anti-HIV indolyl aryl sulfones. *J. Enzym. Inhib. Med. Chem.* 2008; **23**, 980-95.

[12] L Saghaie, H Sakhi, H Sabzyan, M Shahlaei and D Shamshirian. Stepwise MLR and PCR QSAR study of the pharmaceutical activities of antimalarial 3-hydroxypyridinone agents using B3LYP/6-311++ G** descriptors. *Med. Chem. Res.* 2013; **22**, 1679-88

[13] H Kubinyi. QSAR and 3D QSAR in drug design part 1: Methodology. *Drug Discov. Today* 1997; **2**, 457-67.

[14] A Nagpal and SK Paliwal. QSAR model development using MLR, PLS and NN approach to elucidate the physicochemical properties responsible for neurologically important JNK3 inhibitory activity. *J. Pharmaceut. Sci. Res.* 2017; **9**, 1831-43.

[15] D Kim, SI Hong and DS Lee. The quantitative structure-mutagenicity relationship of polycylic aromatic hydrocarbon metabolites. *Int. J. Mol. Sci.* 2006; **7**, 556-70.

[16] A Tropsha and A Golbraikh. Predictive QSAR modeling workflow, model applicability domains, and virtual screening. *Curr. Pharmaceut. Des.* 2007; **13**, 3494-504.

[17] A Tropsha, P Gramatica and VK Gombar. The importance of being earnest: validation is the absolute essential for successful application and interpretation of QSPR models. *QSAR Combin. Sci.*

2003; **22**, 69-77.
[18] N Tripathi, S Paliwal, S Sharma, K Verma, R Gururani, A Tiwari, A Verma, M Chauhan, A Singh, D Kumar and A Pant. Discovery of novel soluble epoxide hydrolase inhibitors as potent vasodilators. *Sci. Rep.* 2018; **8**, 14604.
[19] LD Pennington, MD Bartberger, MD Croghan, KL Andrews, KS Ashton, MP Bourbeau, J Chen, S Chmait, R Cupples, C Fotsch, J Helmering, H Fang-Tsao, RW Hungate, SR Jordan, K Kong, L Liu, K Michelsen, C Moyer, N Nishimura, MH Norman, ..., DJSJ Jr. Discovery and structure-guided optimization of diarylmethanesulfonamide disrupters of glucokinase-glucokinase regulatory protein (GK-GKRP) binding: strategic use of a N→ S (nN→ σ* S–X) interaction for conformational constraint. *J. Med. Chem.* 2015; **58**, 9663-79.
[20] MO Taha, M Habash and MA Khanfar. The use of docking-based comparative intermolecular contacts analysis to identify optimal docking conditions within glucokinase and to discover of new GK activators. *J. Comput. Aided Mol. Des.* 2014; **28**, 509-47.
[21] T Beck and BG Miller. Structural basis for regulation of human glucokinase by glucokinase regulatory protein. *Biochemistry* 2013; **52**, 6232-9.
[22] EI Edache, A Uzairu, PA Mamza and AG Shallangwa. 2D-QSAR, 3D-QSAR, molecular docking, and molecular dynamics simulations in the probe of novel type I diabetes treatment. *Int. J. New Chem.* 2021, https://doi.org/10.22034/ijnc.2021.529335.1161
[23] S Jain, A Bisht, K Verma, S Negi, S Paliwal and S Sharma. The role of fatty acid amide hydrolase enzyme inhibitors in Alzheimer's disease. *Cell Biochem. Funct.* 2022; **40**, 106-17.